Cancer Research

A Hyaluronidase-Responsive Nanoparticle-Based Drug Delivery System for Targeting Colon Cancer Cells

Mingzhen Zhang[1,2], Changlong Xu[1,2,3], Liuqing Wen[4], Moon Kwon Han[1,2], Bo Xiao[1,2], Jun Zhou[4], Yuchen Zhang[1,2], Zhan Zhang[1,2], Emilie Viennois[1,2], and Didier Merlin[1,2,5]

Abstract

The ability of nanoparticles to target tumors and to enable site-specific drug release provides a unique system for the delivery of effective therapy with reduced toxic side effects. In this study, we used mesoporous silica nanoparticles (MSN) to fabricate a targeted drug delivery system that is responsive to hyaluronidase (HAase). Following engraftment of desthiobiotin onto the surface of MSN, a streptavidin complex was generated, which was functionalized with biotin-modified hyaluronic acid (HA) to enable controlled drug release at cancer cells expressing HAase. Various technologies were used to confirm the successful fabrication of this MSN-based nanocarrier system for targeted drug delivery. *In vitro* analyses showed that the release of doxorubicin hydrochloride (Dox) was accelerated significantly in the presence of biotin or HAase and accelerated further in the presence of biotin and HAase. Uptake by cancer cells was mediated efficiently by CD44 receptor–mediated endocytosis and the MSN exhibited good biocompatibility *in vitro* and *in vivo*. MSN-HA/Dox nanoparticles induced apoptosis in cancer cells more efficiently than free doxorubicin and inhibited tumor growth with minimal systemic toxicity *in vivo*. Collectively, our findings offered a preclinical proof of concept for a novel targeted drug delivery carrier system for cancer therapy. *Cancer Res; 76(24); 7208–18. ©2016 AACR.*

Introduction

Malignant tumors are worldwide threats to human health (1). The traditional anticancer strategies, such as chemotherapy, do not distinguish cancerous cells from the healthy cells and, thus, may have poor therapeutic effect on tumors while inflicting collateral damage to healthy cells (2). To address this formidable challenge, diverse classes of nanotechnology-based drug delivery systems (DDS) have been designed. These efforts have shown great promise for improving cancer treatment. The reported DDSs have involved polymeric nanoparticles (3), liposomes (4), dendrimers (5), inorganic nanoparticles (6), and protein nanoparticles (7). Some of these delivery vehicles take advantage of the enhanced permeability and retention effect, through which drugs passively accumulate in tumors due to the leakiness of the vasculature surrounding the mass (8). However, this passive approach is limited by its overdependence on the degree of tumor vascularization and angiogenesis (9, 10), and the high interstitial fluid pressure of solid tumors can work against the successful uptake and homogenous distribution of the drug (10).

As an alternative strategy, researchers have modified delivery vehicles with targeting ligands, such as polysaccharides, antibodies, proteins, and aptamers (6), which should enable active targeting ability via binding to cognate receptors that are overexpressed by cancer cells or angiogenic endothelial cells (11). In this approach, a targeting moiety attached to the surface of DSS may act as a homing device, thereby improving the selective delivery of the loaded drug to specific tissues/cells. In addition to targeting, a DDS should enable the controlled release of drug molecules with a proper behavior to achieve an effective local concentration (12). However, entrapped drug molecules often leak from the delivery vehicles upon their introduction to aqueous solution. To maximize cancer cell death and minimize metastatic spread, a DDS should therefore combine cancer cell targeting with controlled intracellular drug release (13).

Among the reported DDSs, mesoporous silica nanoparticles (MSN) have emerged as robust vehicles for drug delivery. MSNs have many unique and beneficial properties, including well-defined pore structures, excellent biocompatibility, a tunable pore size, and an easily functionalized surface (14, 15). Moreover, the same MSN surface can be simultaneously assembled with multiple different moieties, such as a stimulus-responsive moiety and a targeting moiety. Many stimulus-responsive MSN-based DDSs have been designed to respond to various internal and external stimuli, such as pH (16), redox status (14, 15), enzyme activity (17), small molecules (18), light (19), and temperature (20).

Hyaluronic acid (HA) has recently been highlighted as a tumor-targeting moiety. It is composed of *N*-acetylglucosamine and D-glucuronic acid disaccharide units and is generally considered to be a nontoxic and biodegradable natural acidic polysaccharide macromolecule (21). CD44, the cluster of differentiation (CD)

[1]Institute for Biomedical Sciences, Georgia State University, Atlanta, Georgia. [2]Center for Diagnostics and Therapeutics, Georgia State University, Atlanta, Georgia. [3]The 2nd Affiliated Hospital & Yuying Children's Hospital of Wenzhou Medical University, Wenzhou, Zhejiang, P.R. China. [4]Department of Chemistry, Georgia State University, Atlanta, Georgia. [5]Veterans Affairs Medical Center, Decatur, Georgia.

Note: Supplementary data for this article are available at Cancer Research Online (http://cancerres.aacrjournals.org/).

Corresponding Author: Mingzhen Zhang, Georgia State University, 100 Piedmont Avenue, Atlanta, GA 30303. Phone: 404-413-3597; Fax: 404-413-3580; E-mail: mzhang21@gsu.edu

doi: 10.1158/0008-5472.CAN-16-1681

protein, is the main HA-binding receptor. This single-chain transmembrane glycoprotein has a molecular mass of 80 to 250 kDa and is reportedly overexpressed on various tumor cells, including those of ovarian, breast, and colon cancers (22). In addition to its targeting ability, HA has other unique properties, including its large and biocompatible molecular size, which can be used to block the release of a drug, and its ability to be readily degraded to low molecular weight components by HAase after being taken up by cancer cells through receptor-mediated endocytosis (forming the basis for enzyme-responsive release).

Vitamin H, or more commonly known as biotin, is a B-complex vitamin that helps the body convert food (carbohydrates) into a fuel (glucose) used to produce energy. Biotin also helps the body metabolize fats and protein and can generally promote cell growth (23). However, recent work suggested that biotin may be upregulated in some cancer tissues (e.g., colon cancers) compared with normal tissues (24). Desthiobiotin is a modified form of biotin that binds less tightly to streptavidin (SA) than biotin, while still exhibiting excellent binding specificity [dissociation constant (K_d) = 10^{-11} and 10^{-15} mol/L, respectively; ref. 25]. We hypothesized that the affinities of desthiobiotin and biotin toward SA could be combined with the targeting ability and HAase-mediated degradation of HA to develop a new MSN-based DDS that exhibits targeted drug delivery and intracellular dual-stimulus–responsive drug release.

Here, we report a novel multifunctional MSN-based biotin/HAase dual-stimulus–triggered DDS for targeted therapeutic drug delivery *in vitro* and *in vivo*. Doxorubicin hydrochloride (Dox) was investigated as a model anticancer drug. In this system, desthiobiotin–SA complex and HA were employed as "gatekeepers." Briefly, the external surface of each MSN was modified with desthiobiotin molecules; the MSN pores were blocked with SA via the desthiobiotin–SA interaction; and biotin-modified HA was added to further block the pores and endow MSN-HA/Dox with its targeting capability (Fig. 1A). We propose that after MSN-HA/Dox is preferentially taken up by cancer cells through receptor-mediated endocytosis, the HAase-mediated degradation of HA triggers drug release that undergoes further enhancement by the displacement of desthiobiotin by intracellular biotin (Fig. 1B). This targeted drug release induces cell apoptosis and inhibits tumor growth *in vivo*. Our results suggest that the developed MSN may potentially be a promising drug delivery carrier for efficient tumor therapy.

Materials and Methods

Synthesis of desthiobiotin-functionalized MSNs

For MSN-desthiobiotin synthesis, 110 mg propylamine functionalized silica (MSN-NH_2) was dispersed in 10 mL PBS (pH 7.4). Then, 20 mg NHS-desthiobiotin dissolved in 1mL DMSO was added and stirred (1,000 rpm) at room temperature overnight. The mixture was washed with PBS for three times and dried using lyophilizer to yield the desthiobiotin-functionalized MSN (MSN-desthiobiotin).

Synthesis of SA-functionalized MSNs

For MSN-SA synthesis, 10 mg MSN-desthiobiotin was dispersed in 4 mL PBS (pH 7.4). Then, 1 mL SA (1 mg/mL in PBS) was added and allowed to react at room temperature for 2 hours. The mixture was washed with PBS for three times and dried using lyophilizer to yield the SA-functionalized MSN (MSN-SA).

Preparation of MSN-HA DDS

The MSN-desthiobiotin (10 mg, 4 mL in PBS) was added to 5 mL of doxorubicin (1 mg/mL) in PBS (pH 7.4) solution. After stirring about 12 hours, 1 mL SA (1 mg/mL in PBS) was added and allowed to react at room temperature for 2 hours to cap the pores on the mesoporous silica particles. The final mix solution was centrifuged and washed with PBS for three times; the amount of doxorubicin loaded into MSN-desthiobiotin was determined by analyzing the absorbance of supernatant solution. Rhodamine B was loaded by the same protocol. Then, MSN-SA (2.5 mL, 2 mg/mL) was redispersed in PBS, and mono-biotin labeled HA (2 mg in 200 μL PBS) was added to incubate for another 2 hours to obtain hyaluronic acid–modified MSN (MSN-HA), The theoretical capping amount of HA on the surface of MSN was 15 μg/mg MSN.

Cell culture

Macrophage 264.7, HT-29, and Colon-26 cells were cultured to confluency in 75-cm^2 flasks at 37°C in a humidified atmosphere containing 5 % CO_2. HT-29 cells were cultured in McCoy's 5A medium, macrophage 264.7 cells were cultured in DMEM, and Colon-26 cells were culture in RPMI1640 medium (Life Technologies). All these cases were supplemented with penicillin (100 U/mL), streptomycin (100 U/mL), and heat-inactivated FBS (10%; Atlanta Biologicals). All these cell lines were obtained directly from ATCC (2009–2013), where they were tested and authenticated via morphology, and PCR to rule out interspecies and intraspecies contamination.

Animals

Athymic BALB/c nu/nu female mice, C57BL/6, and FVB/NJ female mice (6–8 weeks old) were purchased from The Jackson Laboratory. Mice were housed under specific pathogen-free conditions. All the experiments involving mice were approved by the Institutional Animal Care and Use Committee of Georgia State University (Atlanta, GA).

Statistical analysis

One-way and two-way ANOVA and *t* tests were used to determine statistical significance (*, $P < 0.05$; **, $P < 0.01$; ***, $P < 0.001$).

Results and Discussion

Preparation and characterization of MSN-HA DDS

Propylamine-functionalized MSN (MSN-NH_2; ∼180 nm in diameter) was characterized by a typical hexagonal channel–like mesoporous structure, as confirmed by scanning electron microscope, transmission electron microscope, small-angle X- ray diffraction (Fig. 2A–C), and nitrogen adsorption–desorption isotherms (Supplementary Fig. S1). Consistent with previous reports (26, 27), MSN-NH_2 displayed a homogeneous spherical morphology and had a highly regular mesoporous structure. Investigation confirmed that nanoparticles <200 nm in diameter can circulate in blood for an extended period (28); thus, the characteristics of our developed MSN suggest that they could potentially reach the target via circulation and might be useful carriers for drug delivery.

To construct our MSN-HA DDS, we first conjugated MSN-NH_2 with NHS-activated desthiobiotin molecules, which are known to react efficiently with primary amine groups (-NH_2), such as those

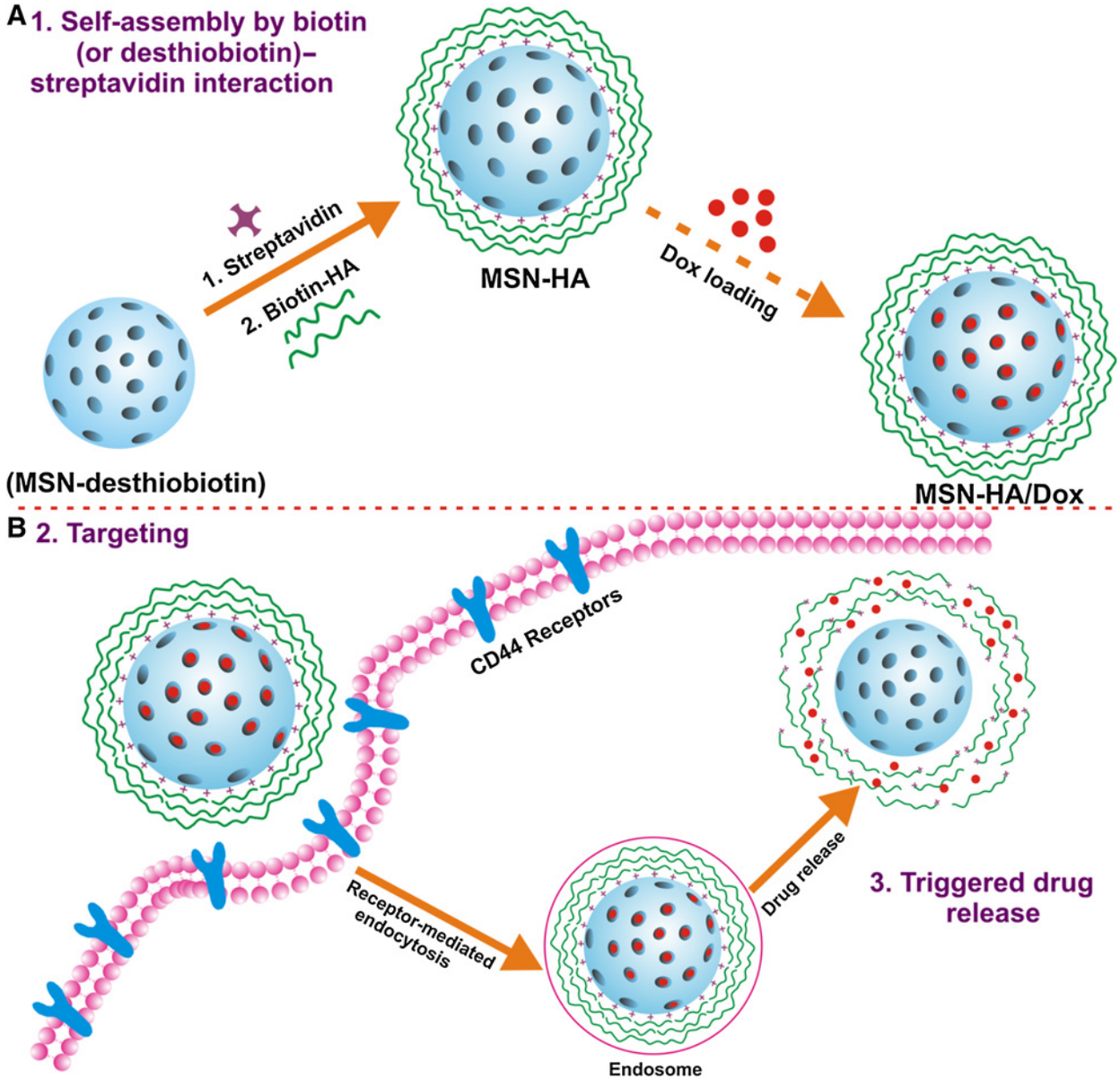

Figure 1.

Schematic diagram to describe MSN-HA nanoparticles mediated delivery of the therapeutic drug, doxorubicin (Dox), to cancer cells. **A,** Drug loading steps to yield MSN-HA/Dox delivery system. Propylamine-functionalized silica (MSN-NH_2) was first modified with desthiobiotin to obtain MSN-desthiobiotin, then by employing biotin (or desthiobiotin)–SA interaction, SA and biotinylated HA were self-assembled on the external surface of MSN to yield MSN-HA. Optionally, therapeutic drug, doxorubicin, was able to load to obtain MSN-HA/Dox. **B,** Schematic illustration of the CD44 receptor–mediated endocytosis and triggering of drug release in tumor cells. MSN-HA/Dox were taken up by cancer cell via receptor-mediated endocytosis (HA–CD44 interaction), then loaded doxorubicin was released from the pore of MSN by the triggering of HAase and intracellular biotin.

on the surface of MSN-NH_2, to form stable amide bonds (23). The efficient conjugation of desthiobiotin with MSN (MSN-desthiobiotin) was validated by the appearance of a broad absorption band at around 1,680 cm^{-1} in the Fourier transform infrared spectra (Supplementary Fig. S2), which can be assigned to vibrations of the cyclic urea group within the attached desthiobiotin molecules. For some experiments, the MSN were loaded with doxorubicin, as a model anticancer drug, or rhodamine B, which was used as a tracer to locate the distributions of MSN within the cells. After doxorubicin was loaded into the pores of MSN-desthiobiotin, SA was added to cap the pores through the desthiobiotin–SA interaction. Desthiobiotin and SA can form a complex that blocks the release of a drug or dye from the pores of a nanoparticle. To provide the SA-capped MSNs with another level of targeting capability and to further cap the pores and prevent drug/dye release, we performed additional functionalization with

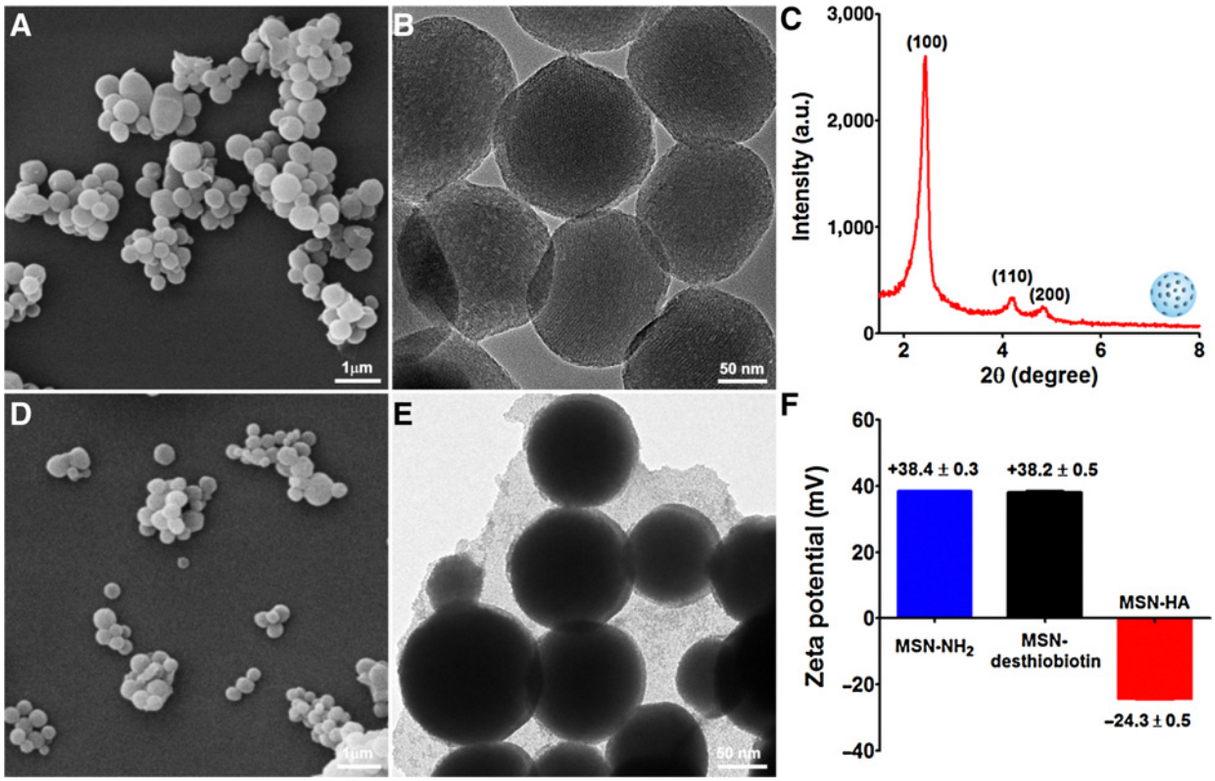

Figure 2.

Characterization of MSN-NH_2 and MSN-HA nanoparticles. **A,** Scanning electron microscope images were performed to characterize MSN-NH_2 nanoparticles; scale bar, 1 μm. **B,** Transmission electron microscope images were performed to characterize MSN-NH_2 nanoparticles; scale bar, 50 nm. **C,** Small-angle power X-ray diffraction was employed to characterize the structure of MSN-NH_2. The high ordered lattice array indicated MSN-NH_2 has a uniform and well-defined mesostructure. **D,** Scanning electron microscope images of MSN-HA; scale bar, 1 μm. **E,** Transmission electron microscope images of MSN-HA; scale bar, 50 nm. **F,** Zeta potentials of MSN-NH_2, MSN-desthiobiotin, and MSN-HA were measured. MSN-NH_2 and MSN-desthiobiotin showed a positive surface charge; after grafting HA, surface charge was changed to negative, indicating the successful link of HA ($n = 3$).

biotin-labeled HA. SEM showed that MSN-HA displayed a spherical morphology similar to that of MSN-NH_2 (Fig. 2D), but the surface modification obscured the mesoporous structure of MSN-HA (Fig. 2E). Zeta potential measurements showed that MSN-HA nanoparticles had a highly negative charge (-24.3 ± 0.5 mV; Fig. 2F) when compared with MSN-NH_2 ($+38.4 \pm 0.3$ mV) and MSN-desthiobiotin ($+38.2 \pm 0.3$ mV), confirming that HA had been successfully linked to the MSN surface. After doxorubicin was loaded to generate MSN-HA/Dox, spectrophotometry revealed a drug-loading content of approximately 5% (w/w), which was comparable with that obtained in a previous study (28). In addition, as shown in Supplementary Fig. S3, MSN-HA/Dox showed low DPI value (0.157) and good dispersibility, indicating that potential aggregation of MSN-HA/Dox did not occur, and therefore, the followed targeted therapeutic efficacy would not be affected. The successful loading of rhodamine B into the pores of MSN-HA was confirmed by fluorescence imaging, as shown in Supplementary Fig. S4.

MSN-HA nanoparticles show biotin- and HAase-dependent drug release

The K_d of biotin toward SA ($K_d \sim 10^{-15}$ mol/L) is about 10,000-fold higher than that of desthiobiotin ($K_d \sim 10^{-11}$ mol/L). In the context of our DDS, biotin will thus replace desthiobiotin within the cell, triggering drug release. To investigate the dual-stimulus–responsive release behavior of our designed MSN-HA DDS, we used biotin and HAase as triggers under conditions that mimicked the tumor microenvironment (pH 6.5). As shown in Fig. 3, MSN/Dox exhibited higher doxorubicin release in pH 6.5 solution when compared with MSN-HA/Dox. The cumulative release of doxorubicin from MSN/Dox was more than 80% by 24 hours. Under the same pH condition, MSN-HA/Dox released only approximately 12% of the loaded doxorubicin, indicating that our use of desthiobiotin–SA complex and polysaccharide-HA yielded good capping. In the presence of biotin or HAase alone, the cumulative drug releases from MSN-HA/Dox were approximately 60% and 40%, respectively, at 24 hours posttreatment. The cumulative drug release was further improved to approximately 70% in the presence of both biotin and HAase. This likely reflects the possible degradation of HA of MSN-HA/Dox by HAase and/or the displacement of desthiobiotin by biotin in cotreated cells compared with those treated with biotin alone. The release profiles of doxorubicin from MSN-HA/Dox under various stimulations in neutral buffer (pH 7.0) were also examined. We obtained release profiles similar to those observed under pH 6.5. Blood and healthy tissues are under neutral pH and express minimal biotin and HAase to trigger the release of doxorubicin from MSN-HA/Dox. Therefore, our smart MSN-HA nanoparticles

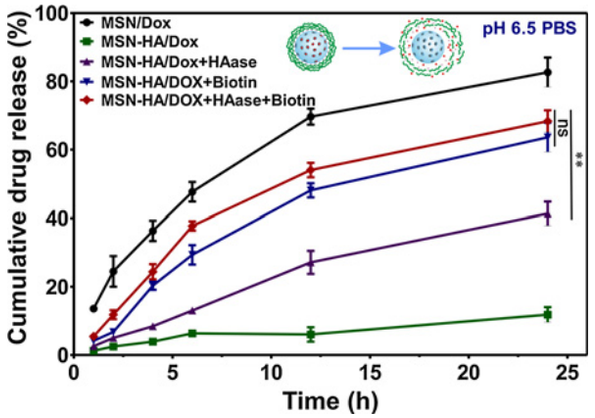

Figure 3.

The biotin- and HAase-responsive release profiles of doxorubicin (Dox) were evaluated. Drug release under pH 6.5 was conducted to mimic the condition of tumor microenvironment. Under different stimulus condition, biotin (2 μmol/L), HAase (150 U/mL), or both were added to MSN-HA/Dox solution; as a control, MSN-Dox was employed. At specified time points (1, 2, 4, 6, 12, and 24 hours), cumulative drug release was measured and compared ($n = 3$). **, $P < 0.01$.

have very good capping efficacy and do not release doxorubicin until they reach the stimulating conditions (i.e., the cancer milieu; Supplementary Fig. S5). Taken together, our results show that MSN-HA/Dox exhibits the highest drug release in the presence of both biotin and HAase under a pH that mimics the tumor microenvironment. Thus, our DDS shows great potential for tumor therapy.

MSN-HA can be taken up efficiently by Colon-26 and HT-29 cells through CD44 receptor–mediated endocytosis

Efficient cellular uptake is a major requirement for the therapeutic efficacy of nanoparticles (3). To test the targeting specificity of MSN-HA, we evaluated the cellular uptake of MSN-HA/rhodamine B by Colon-26 cells and HT-29 cells. Membrane-localized CD44, which is known to be the main HA-binding receptor, is responsible for the interaction between HA and the surface of cancer cells (29). We incubated MSN-HA with Colon-26 and HT-29 cells at 37°C for 4 hours with or without free HA. Subsequent confocal microscopy revealed that cells incubated with MSN-HA alone showed strong fluorescence of rhodamine B, both at the membrane and within the cells (Fig. 4A, a and c). In the presence of free HA, in contrast, we observed less fluorescence from MSN-HA/rhodamine B in both Colon-26 and HT-29 cells (Fig. 4A, b and d). This confirms that MSN-HA were subject to CD44-mediated endocytosis. The cellular uptake of MSN-HA/rhodamine B by Colon-26 and HT-29 cells was also assessed by flow cytometry, which revealed much higher fluorescence in HA-free cultures of Colon-26 (Fig. 4B) and HT-29 cells (Fig. 4C) than in their HA-treated counterparts. Together, our results are consistent with the idea that MSN-HA undergoes CD44 receptor–mediated endocytosis.

To confirm the involvement of receptor-mediated endocytosis, we performed a fluorescence-based colocalization study of MSN-HA/rhodamine B and FITC-labeled transferrin (Tf-FITC). Transferrin is internalized by receptor-mediated endocytosis via the formation of clathrin-coated pits and is widely used as a tracker for clathrin-dependent endocytosis. Consistent with the results of our confocal microscopic and flow cytometric analyses, both Colon-26 and HT-29 cells showed high levels of colocalization between MSN-HA/rhodamine B (red color; Supplementary Fig. S6) and Tf-FITC (arrows, yellow color).

Evaluation the biocompatibility of MSN-HA, both *in vitro* and *in vivo*

For a potential DDS, biocompatibility is a key issue that should be investigated. To assess the biocompatibility of MSN-HA, we first used MTT assays to quantify the viability of cells treated with different concentrations of MSN and MSN-HA. Colon-26 and HT-29 cells treated with MSN-HA showed higher cell viability than those treated with the same concentrations of MSN at up to the highest tested dose of 200 μg/mL (Supplementary Fig. S7A and S7B), indicating that HA modification improved the biocompatibility of MSN. An ATPLite assay, which quantitatively measures cell proliferation, confirmed these results (Supplementary Fig. S7C and S7D). These results indicate that MSN-HA has good biocompatibility *in vitro*.

Next, we explored the biocompatibility of MSN-HA *in vivo*. Intravenous injection of mice with MSN-HA (1 mg/100 μL) daily for 7 days did not trigger any change in the weights/body weights of the heart, liver, spleen, lung, or kidney (Supplementary Fig. S8A). Histologic analysis of hematoxylin and eosin (H&E)-stained tissue sections did not find any clear evidence of organ damage in the MSN-HA group compared with the control group. The liver hepatocytes appeared normal, no myocardial fibrillary loss or vacuolation was observed in the heart, no pulmonary fibrosis was detected in lung samples, and no necrosis was observed in any analyzed samples (Supplementary Fig. S8B). We also failed to observe any significant increase in the indicators of liver injury, alanine aminotransferase (ALT), or aspartate aminotransferase (AST), in the MSN-HA group compared with the control group (Supplementary Fig. S8C). Collectively, these findings indicate that MSN-HA exhibits higher biocompatibility both *in vitro* and *in vivo* and therefore should be useful as a safe drug delivery platform.

Nuclear transport of doxorubicin and subsequent cell apoptosis

Research showed that doxorubicin can diffuse into nuclei, where it interacts with DNA molecules (30). As shown in Supplementary Fig. S9, free doxorubicin or MSN-HA/Dox-released doxorubicin was transported into nuclei after 8-hour incubation, indicating that MSN-HA/Dox can successfully be taken up and deliver doxorubicin into the nucleus to exert its function.

To compare the apoptosis induced by free doxorubicin and MSN-HA/Dox, we used Annexin V-FITC and propidium iodide (PI) double staining to examine treated Colon-26 and HT-29 cells. Fluorescence microscopy revealed that free doxorubicin- and MSN-HA/Dox–treated Colon-26 cells showed positive staining for both Annexin V-FITC and PI (Fig. 5A), whereas no such signal was detected from untreated control cells. Flow cytometry–based quantification revealed apoptotic cell populations of 90.8 ± 5.5%, 41.8 ± 9.2%, and 3.2 ± 2.1% in MSN-HA/Dox-treated, free doxorubicin-treated, and control cells, respectively (Fig. 5B and C). Similar results were obtained in HT-29 cells, which exhibited apoptotic populations of 90.7 ± 1.5%, 50.2 ± 5.6%, and 1.1 ± 0.9%, respectively (Supplementary Fig. S10). We also compared

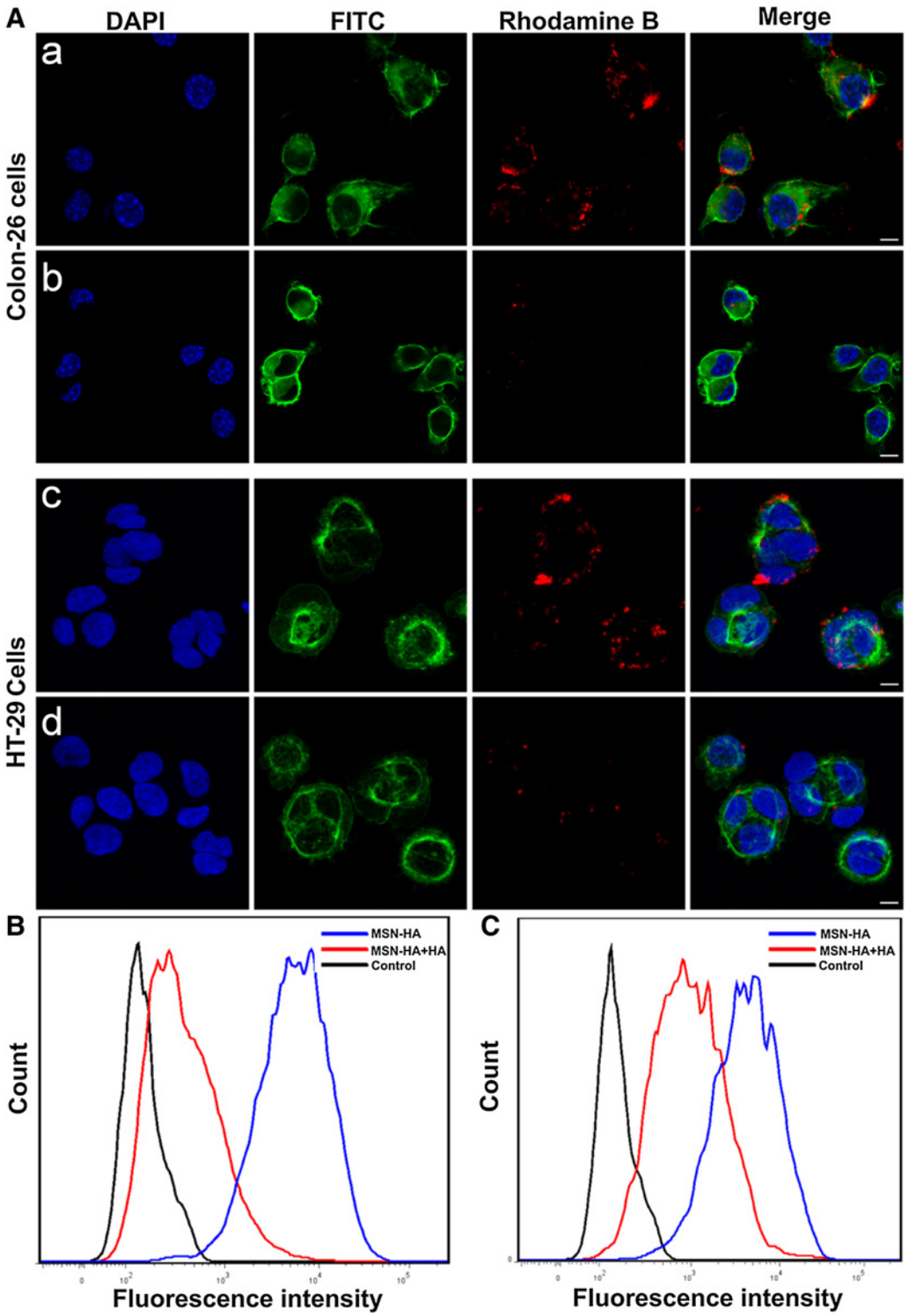

Figure 4.

Endocytosis pathway of MSN-HA taken up by Colon-26 and HT-26 cells was investigated. **A,** Confocal microscopic images show: **a,** Colon-26 cells treated with MSN-HA in the absence of HA; **b,** Colon-26 cells treated with MSN-HA in the presence of HA (2 mg/mL); **c,** HT-29 cells treated with MSN-HA in the absence of HA; **d,** HT-29 cells treated with MSN-HA in the presence of HA (2 mg/mL). Blue channel, DAPI; green channel, FITC; red channel, the fluorescence of rhodamine. **B,** The fluorescence intensities of rhodamine B–labeled MSN-HA applied with or without HA were quantified by flow cytometry. **B,** Colon-26 cells. **C,** HT-29 cells. ($n = 5$). Scale bar, 20 μm.

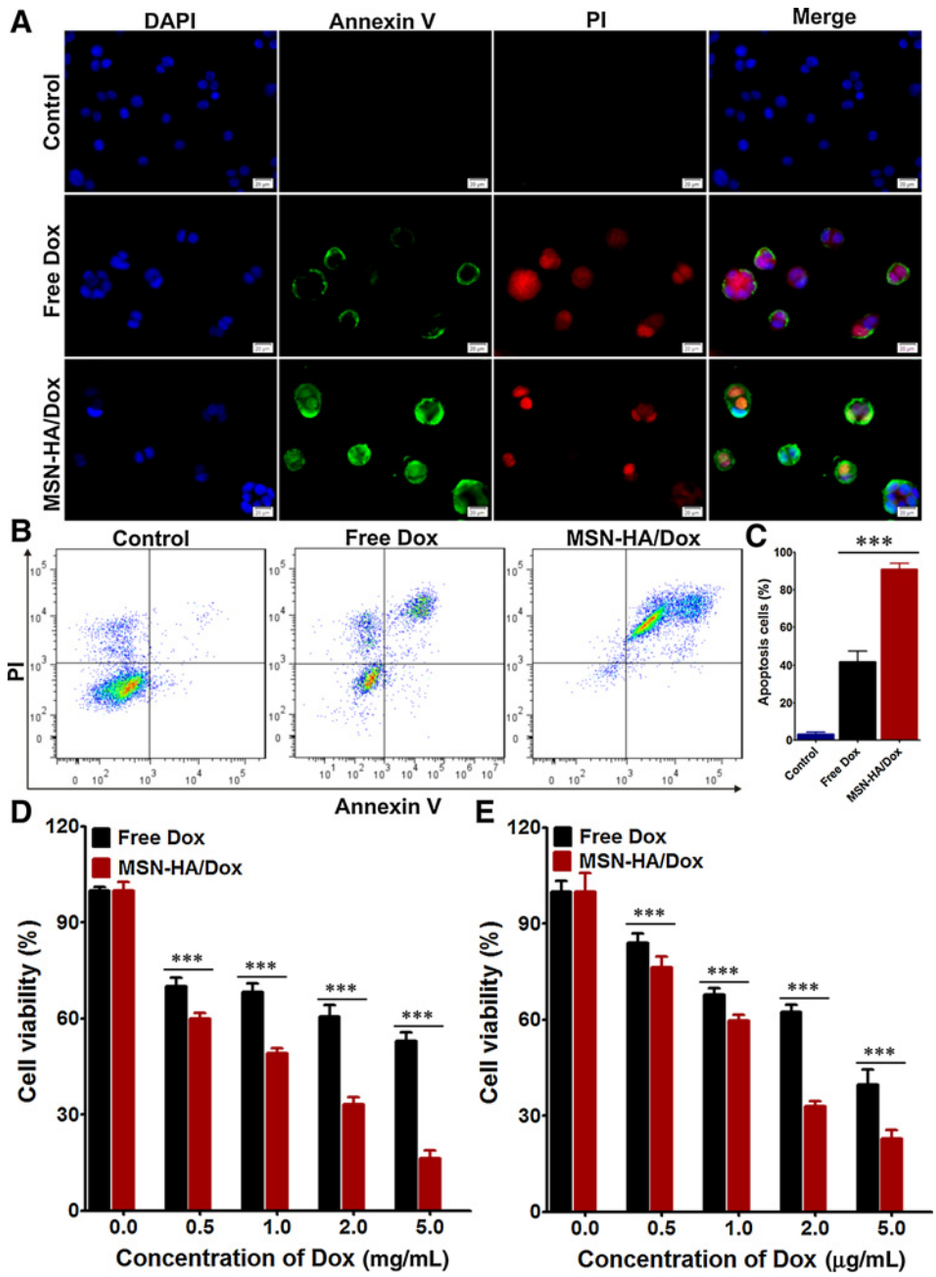

Figure 5.
Evaluation of the apoptosis induced by MSN-HA/Dox *in vitro*. **A,** Fluorescence imaging of Colon-26 cells treated with free doxorubicin (Dox) or MSN-HA/Dox for 8 hours and then costained with Annexin V-FTIC and PI. Scale bar, 20 μm. **B,** Flow cytometric analysis of apoptosis in Colon-26 cells treated with free doxorubicin or MSN-HA/Dox for 8 hours. **C,** Quantification of the Annexin V-FTIC/PI-positive apoptotic cells from **B**. Data are from three independent experiments. **D,** The apoptotic effects of free doxorubicin and MSN-HA/Dox in Colon-26 cells were assessed by MTT assay, ($n = 5$). **E,** The apoptotic effects of free doxorubicin and MSN-HA/Dox in HT-29 cells were assessed by MTT assay ($n = 5$). ***, $P < 0.001$.

apoptosis using 3-(4,5-dimethylthiazol-2-yl)-2,5-diphenyltetrazolium bromide (MTT) assays. As shown in Fig. 5D and E, MSN-HA/Dox induced more cell apoptosis than free doxorubicin at all tested concentrations (0.5, 1.0, 2.0, and 5.0 μg/mL doxorubicin) in both Colon-26 and HT-29 cells. These results confirmed that MSN-HA/Dox has a higher therapeutic effect than free doxorubicin. Consequently, MSN-HA/Dox could improve the therapeutic effect of doxorubicin and might serve as a good DDS.

MSN-HA shows relatively little nonspecific interaction with proteins, blood cells, and macrophages

After a nanoparticle enters the circulation, the first biological event is the adsorption of the abundant plasma proteins onto to the nanoparticle surface (31). This would be expected to change the surface characteristics of a nanoparticle-based DDS and impact its delivery efficiency *in vivo*. To investigate the interaction of MSN-SA with such proteins, we followed previous studies by using BSA (15), which is a major serum protein often found in the protein corona of nanoparticles. As shown in Supplementary Fig. S11A, significantly less BSA was absorbed by MSN-HA compared with MSN at both 12 and 24 hours. This suggests that the surface-bound HA prevents proteins from adsorbing into the MSN, which could prolong the circulation time of our DDS in the blood (32).

In blood, the hemolysis by nanoparticles seriously limits the *in vivo* application of nanoparticle-based DDS (33, 34). In our studies, however, although Triton X-100 (positive control)

achieved 100% hemolysis, MSN-HA did not trigger hemolysis at concentrations up to 1 mg/mL (Supplementary Fig. S11B). This suggests that intravenously administered MSN-HA could be nontoxic toward erythrocytes.

When nanoparticles enter a host, they firstly interact with macrophages to trigger immune responses, such as inflammation. Prominent inflammatory mediators, IL6, IL1β, and TNFα, are typically used as markers of an acute macrophage-related inflammatory response (35). As shown in Supplementary Fig. S12A–S12C, the mRNA levels of IL6, IL1β, and TNFα were significantly lower in MSN-HA–treated RAW 264.7 cells (a macrophage cell line) than in MSN-treated cells. To further investigate the immunologic effect of MSN-HA/Dox *in vivo*, we subjected mice to single-dose injections of MSN-HA/Dox and obtained sera at 24 and 48 hours postinjection. As shown in Supplementary Fig. S12D–S12F, the protein concentrations of IL6, IL1β, and TNFα were not significantly different between MSN-HA/Dox-injected and control mice at 24 and 48 hours, indicating that HA capping of MSN reduced the likelihood of triggering a macrophage-induced inflammatory response. These observations reflect the improvement of the biocompatibility of MSN via the conjugation of HA, thereby reducing the inflammatory response triggered by our MSN-HA delivery system.

Antitumor effects of MSN-HA/Dox *in vivo*

To evaluate the antitumor effects of MSN-HA/Dox *in vivo*, we established a Colon-26 xenograft tumor model in athymic BALB/c nu/nu mice. The tumor-bearing mice were randomly divided into four groups and intravenously injected with saline, MSN-HA, free doxorubicin, or MSN-HA/Dox. As shown in Fig. 6A, visual observations indicated that the MSN-HA/Dox–treated mice showed the most efficient reduction of tumor size. The saline- and MSN-HA–treated control groups exhibited similar tumor volumes at the end of the experiment (Fig. 6B), whereas the free doxorubicin-treated group showed slightly decreased tumor growth compared with the control groups (Fig. 6B). At the end of the experiment, tumor weights were compared. As shown in Fig. 6C, the MSN-HA/Dox-treated group showed the lowest tumor weight, which was significantly lower than that of the free doxorubicin–treated group. The saline- and MSN-HA–treated control groups displayed similar tumor weights, indicating similar tumor growth.

These findings, which are consistent with the results of our *in vitro* apoptosis assays, indicate that MSN-HA/Dox shows better tumor growth inhibition than free doxorubicin *in vivo*. This may reflect that free doxorubicin quickly diffuses into tissues and organs following intravenous injection (31), potentially affecting normal tissues and decreasing the amount of free drug that would reach the tumor site. Moreover, free doxorubicin has a short half-life *in vivo* and is quickly cleared from the body (36).

To explore the mechanism underlying the tumor growth inhibition conferred by our DDS, we performed terminal deoxynucleotidyl transferase dUTP nick-end labeling (TUNEL) apoptosis assays. As shown in Fig. 6D, few TUNEL-positive apoptotic cells (green dots) were detected in tumor sections from the saline- and MSN-HA–treated groups, providing additional evidence that MSN-HA shows good biocompatibility *in vivo*. In contrast, tumor tissues from the MSN-HA/Dox-treated group showed the most severe apoptosis among the different groups, indicating that MSN-HA/Dox inhibits the growth of solid tumor model by inducing apoptosis.

To further confirm the improved therapeutic efficacy of MSN-HA/Dox, we performed histologic analysis of tumor tissues. H&E staining and subsequent analysis (Supplementary Fig. S13) revealed that sections from the MSN-HA/Dox-treated group harbored significantly fewer cancerous cells than those from the saline-, MSN-HA-, and free doxorubicin-treated groups.

To investigate the potential side effects of MSN-HA/Dox, we performed histologic examinations of major organs (heart, liver, spleen, lung, and kidney) at the end of the experiment. As shown in Fig. 7, mice of the control and MSN-HA/Dox groups did not show any noticeable signs of tissue or cellular damage in the examined tissues (e.g., myocardial fibrillar loss or vacuolation in the heart; edema, ballooning, and/or degeneration of hepatocytes; increased numbers of granulocytes in the spleen; tubular vacuolization or tubular dilation with hemorrhagic areas in the kidney; or increased alveolar wall thickness or cellular infiltration in the lung). In contrast, free doxorubicin induced typical myocardial damage with intensive vacuolization and myofibril loss (Fig. 7, blue circles).

To investigate time-dependent biodistribution of our DDS, we administered a single dose of MSN-HA/near-infrared dye (DiR) to mice via intravenous injection. No postinjection abnormality was observed in the eating, drinking, grooming, activity, exploratory behavior, urination, or neurologic status of treated mice. At 4, 24 hours, and 7 days postinjection, mice were sacrificed and the DiR contents were measured in different organs (heart, liver, spleen, lung, and kidney) using an IVIS *in vivo* imaging system. As shown in Supplementary Fig. S14, MSN-HA/DiR was predominately found in organs of the reticuloendothelial system (liver and spleen) at 4 and 24 hours postinjection. The dye was noticeably cleared from the body within one week. This biodistribution reflects that the protective HA layer on the surface of the MSN nanoparticles prevented this DDS from being recognized and engulfed by phagocytes of the liver and spleen, thereby reducing the cellular uptake by liver and spleen. These results suggest that MSN-HA/Dox could have a low toxicity to the body and could thus be suitable for use as a real anticancer system *in vivo*. Our findings in this regard are consistent with those of the previous studies (16, 31, 37).

On the basis of the results presented in this report, we conclude that our biotin/HAase dual-responsive mesoporous silica DDS (MSN-HA/Dox) exhibits better selective antitumor effects against solid tumors than free doxorubicin. Mechanistically, these effects reflect that (i) the HA on the surface of MSN-HA/Dox uses active targeting to improve the selective delivery of the loaded drug to tumor tissues; (ii) the capping of the pores alleviates the premature release of highly toxic anticancer drugs during the delivery process; and (iii) extracellular matrix–localized HAase and intracellular biotin both trigger the release of the encapsulated doxorubicin, improving its antiproliferative activity in a solid cancer. As the zeta potential of MSN-HA/Dox was highly negative, it is reasonable to believe that the nanoparticles escape from the endosome to interact with biotin in the cytoplasm (23).

In conclusion, we herein designed and constructed a biotin and hyaluronidase dual-responsive DDS (MSN-HA/Dox) for a targeted therapeutic drug delivery *in vitro* and *in vivo*. Desthiobiotin-modified MSN was used as the initial carrier to load doxorubicin. The polysaccharide, hyaluronic acid, was grafted onto the MSN surface via the biotin–streptavidin interaction to serve as a targeting moiety. The pores of this delivery system were capped by desthiobiotin/streptavidin complexes and HA to eliminate

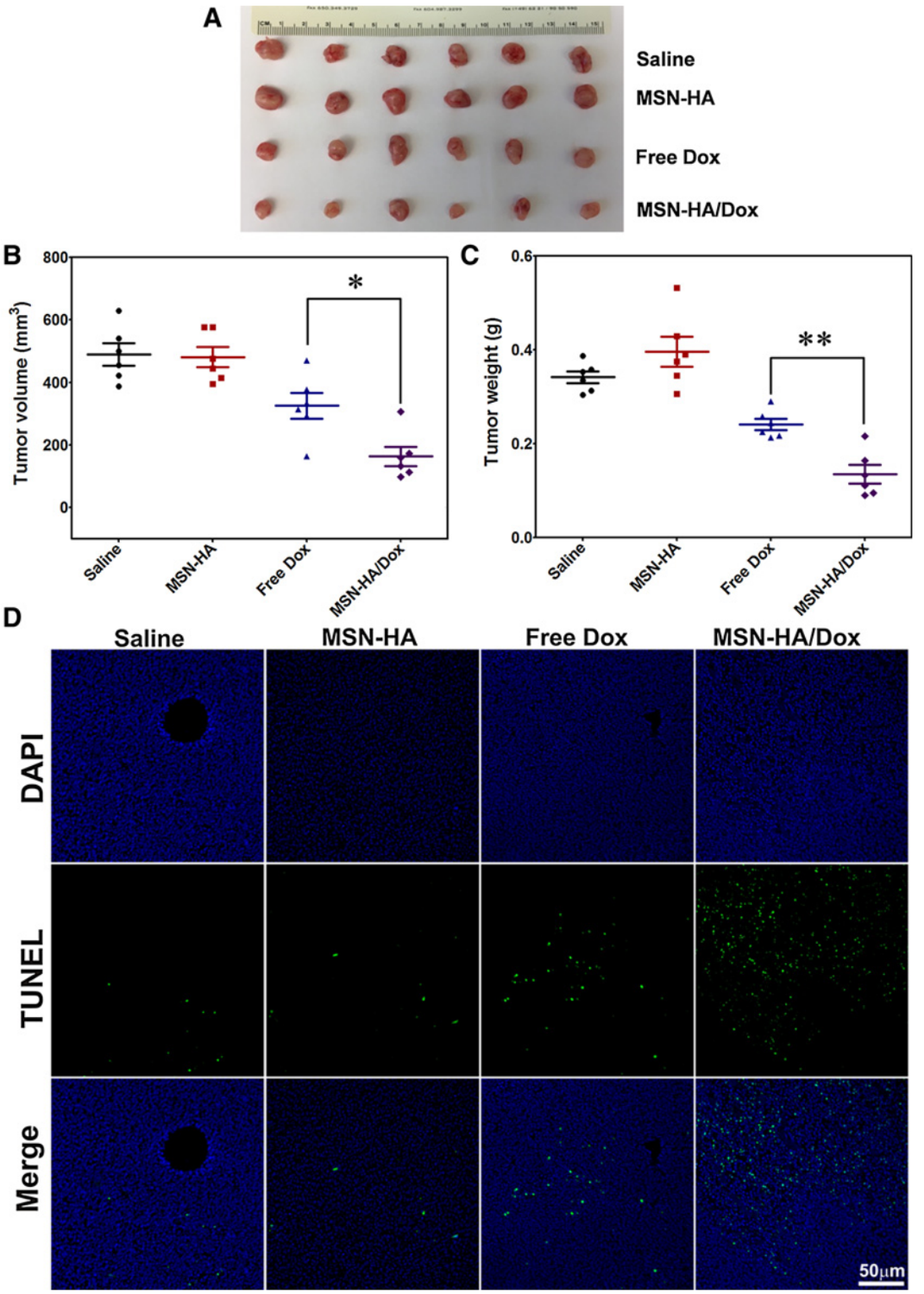

Figure 6.

Effects of MSN-HA/Dox against Colon-26 xenograft tumors were evaluated *in vivo*. **A,** Representative photos of tumor tissues obtained from tumor-bearing mice treated for 18 days with saline (control), MSN-HA, free doxorubicin (Dox), or MSN-HA/Dox ($n = 6$). **B,** Tumor volumes were measured at the end of the experiment ($n = 6$). **C,** Tumor weights were measured at the end of the experiment ($n = 6$). **D,** TUNEL staining was used to examine apoptosis in tumor sections (green, TUNEL-positive cells; blue, cell nuclei; $n = 4$). Scale bar, 50 μm; *, $P < 0.05$ and **, $P < 0.01$.

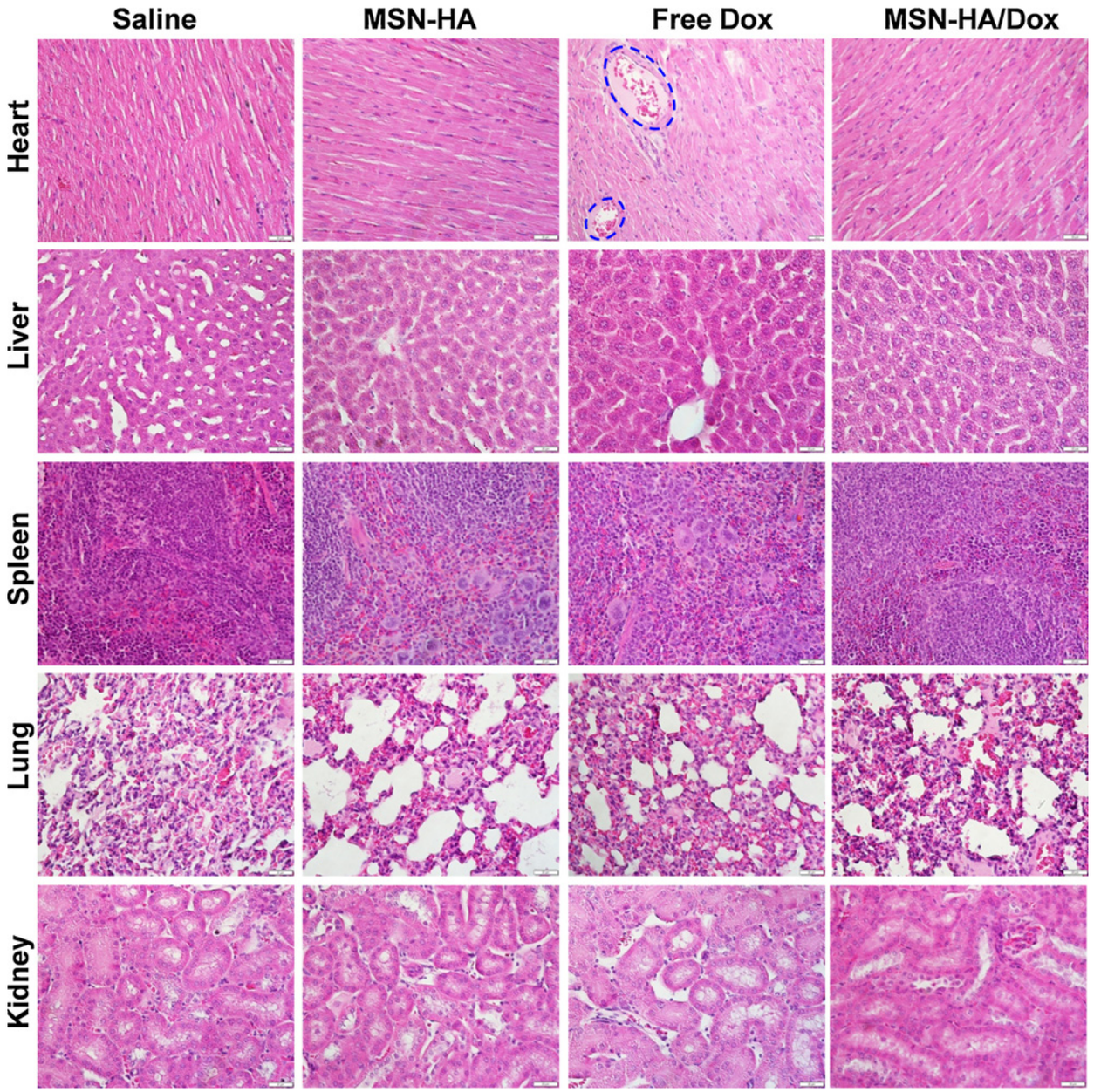

Figure 7.
The major organs of tumor-bearing mice treated with saline, MSN-HA, free doxorubicin (Dox), or MSN-HA/Dox were subjected to histologic examination. Heart samples of free doxorubicin-treated mice show intensive vacuolization and myofibril loss (as indicated). Scale bar, 20 μm.

the premature drug leakage. Following uptake of the nanoparticles by target cells, HAase in the extracellular matrix and biotin in the cytoplasm opened the pores for controlled intracellular release of the entrapped drug. MSN-HA/Dox triggered enhanced apoptosis among cancer cells *in vitro* and conferred better antitumor effects *in vivo* compared with the free drug. Our findings suggest that this novel DDS may hold promise for efficient tumor therapy.

Disclosure of Potential Conflicts of Interest

No potential conflicts of interest were disclosed.

Authors' Contributions

Conception and design: M. Zhang, B. Xiao, D. Merlin
Development of methodology: Z. Zhang, D. Merlin
Acquisition of data (provided animals, acquired and managed patients, provided facilities, etc.): M. Zhang, C. Xu, J. Zhou
Analysis and interpretation of data (e.g., statistical analysis, biostatistics, computational analysis): M. Zhang, L. Wen, E. Viennois
Writing, review, and/or revision of the manuscript: M. Zhang, L. Wen, M.K. Han, B. Xiao, Y. Zhang, E. Viennois, D. Merlin
Administrative, technical, or material support (i.e., reporting or organizing data, constructing databases): Y. Zhang, D. Merlin
Study supervision: D. Merlin

Grant Support

This work was supported by grants from the Department of Veterans Affairs BX002526) and the National Institutes of Health of Diabetes and Digestive and Kidney (RO1-DK-071594 to D. Merlin). M. Zhang and E. Viennois are recipients of a Research Fellowship Award from the Crohn's & Colitis Foundation of America. D. Merlin is a recipient of a Research Career Scientist Award from the Department of Veterans Affairs.

Received June 18, 2016; revised September 8, 2016; accepted September 26, 2016; published OnlineFirst October 14, 2016.

References

1. Thun MJ, DeLancey JO, Center MM, Jemal A, Ward EM. The global burden of cancer: priorities for prevention. Carcinogenesis 2010;31:100–10.
2. Brigger I, Dubernet C, Couvreur P. Nanoparticles in cancer therapy and diagnosis. Adv Drug Deliv Rev 2012;64:24–36.
3. Xiao B, Zhang M, Viennois E, Zhang Y, Wei N, Baker MT, et al. Inhibition of MDR1 gene expression and enhancing cellular uptake for effective colon cancer treatment using dual-surface-functionalized nanoparticles. Biomaterials 2015;48:147–60.
4. Wei T, Liu J, Ma H, Cheng Q, Huang Y, Zhao J, et al. Functionalized nanoscale micelles improve drug delivery for cancer therapy *in vitro* and *in vivo*. Nano Lett 2013;13:2528–34.
5. Kanamala M, Wilson WR, Yang M, Palmer BD, Wu Z. Mechanisms and biomaterials in pH-responsive tumour targeted drug delivery: a review. Biomaterials 2016;85:152–67.
6. Baeza A, Colilla M, Vallet-Regí M. Advances in mesoporous silica nanoparticles for targeted stimuli-responsive drug delivery. Expert Opin Drug Deliv 2015;12:319–37.
7. Murata M, Narahara S, Kawano T, Hamano N, Piao JS, Kang J-H, et al. Design and function of engineered protein nanocages as a drug delivery system for targeting pancreatic cancer cells via neuropilin-1. Mol Pharm 2015;12:1422–30.
8. Prabhakar U, Maeda H, Jain RK, Sevick-Muraca EM, Zamboni W, Farokhzad OC, et al. Challenges and key considerations of the enhanced permeability and retention effect for nanomedicine drug delivery in oncology. Cancer Res 2013;73:2412–17.
9. Keereweer S, Mol IM, Kerrebijn JD, Van Driel PB, Xie B, de Jong B, et al. Targeting integrins and enhanced permeability and retention (EPR) effect for optical imaging of oral cancer. J Surg Oncol 2012;105:714–18.
10. Doleschel D, Rix A, Arns S, Palmowski K, Gremse F, Merkle R, et al. Erythropoietin improves the accumulation and therapeutic effects of carboplatin by enhancing tumor vascularization and perfusion. Theranostics 2015;5:905.
11. Salvati A, Pitek AS, Monopoli MP, Prapainop K, Bombelli FB, Hristov DR, et al. Transferrin-functionalized nanoparticles lose their targeting capabilities when a biomolecule corona adsorbs on the surface. Nat Nanotechnol 2013;8:137–43.
12. Weiser JR, Saltzman WM. Controlled release for local delivery of drugs: barriers and models. J Control Release 2014;190:664–73.
13. Yin Q, Shen J, Zhang Z, Yu H, Li Y. Reversal of multidrug resistance by stimuli-responsive drug delivery systems for therapy of tumor. Adv Drug Deliv Rev 2013;65:1699–715.
14. Zhao Q, Liu J, Zhu W, Sun C, Di D, Zhang Y, et al. Dual-stimuli responsive hyaluronic acid-conjugated mesoporous silica for targeted delivery to CD44-overexpressing cancer cells. Acta Biomater 2015;23:147–56.
15. Zhao Q, Geng H, Wang Y, Gao Y, Huang J, Wang Y, et al. Hyaluronic acid oligosaccharide modified redox-responsive mesoporous silica nanoparticles for targeted drug delivery. ACS Appl Mater Interfaces 2014;6:20290–99.
16. Chen Y, Ai K, Liu J, Sun G, Yin Q, Lu L. Multifunctional envelope-type mesoporous silica nanoparticles for pH-responsive drug delivery and magnetic resonance imaging. Biomaterials 2015;60:111–20.
17. Aznar E, Villalonga R, Giménez C, Sancenón F, Marcos MD, Martínez-Máñez R, et al. Glucose-triggered release using enzyme-gated mesoporous silica nanoparticles. Chem Commun 2013;49:6391–93.
18. Wang Y, Zhao Q, Han N, Bai L, Li J, Liu J, et al. Mesoporous silica nanoparticles in drug delivery and biomedical applications. Nanomedicine 2015;11:313–27.
19. Yang X, Liu X, Liu Z, Pu F, Ren J, Qu X. Near-infrared light-triggered, targeted drug delivery to cancer cells by aptamer gated nanovehicles. Adv Mater 2012;24:2890–95.
20. Shang L, Bian T, Zhang B, Zhang D, Wu LZ, Tung CH, et al. Graphene-supported ultrafine metal nanoparticles encapsulated by mesoporous silica: robust catalysts for oxidation and reduction reactions. Angew Chem Int Ed 2014;53:250–54.
21. Choi KY, Yoon HY, Kim J-H, Bae SM, Park R-W, Kang YM, et al. Smart nanocarrier based on PEGylated hyaluronic acid for cancer therapy. ACS Nano 2011;5:8591–99.
22. Dosio F, Arpicco S, Stella B, Fattal E. Hyaluronic acid for anticancer drug and nucleic acid delivery. Adv Drug Deliv Rev 2016;97:204–36.
23. Li L-L, Xie M, Wang J, Li X, Wang C, Yuan Q, et al. A vitamin-responsive mesoporous nanocarrier with DNA aptamer-mediated cell targeting. Chem Commun 2013;49:5823–25.
24. Russell-Jones G, McTavish K, McEwan J, Rice J, Nowotnik D. Vitamin-mediated targeting as a potential mechanism to increase drug uptake by tumours. J Inorg Biochem 2004;98:1625–33.
25. Chivers CE, Crozat E, Chu C, Moy VT, Sherratt DJ, Howarth M. A streptavidin variant with slower biotin dissociation and increased mechanostability. Nat Methods 2010;7:391–93.
26. Zhang J, Yuan Z-F, Wang Y, Chen W-H, Luo G-F, Cheng S-X, et al. Multifunctional envelope-type mesoporous silica nanoparticles for tumor-triggered targeting drug delivery. J Am Chem Soc 2013;135:5068–73.
27. Muhammad F, Guo M, Qi W, Sun F, Wang A, Guo Y, et al. pH-triggered controlled drug release from mesoporous silica nanoparticles via intracelluar dissolution of ZnO nanolids. J Am Chem Soc 2011;133:8778–81.
28. Liu J, Zhang B, Luo Z, Ding X, Li J, Dai L, et al. Enzyme responsive mesoporous silica nanoparticles for targeted tumor therapy in vitro and in vivo. Nanoscale 2015;7:3614–26.
29. Götte M, Yip GW. Heparanase, hyaluronan, and CD44 in cancers: a breast carcinoma perspective. Cancer Res 2006;66:10233–37.
30. Sui M, Liu W, Shen Y. Nuclear drug delivery for cancer chemotherapy. J Control Release 2011;155:227–36.
31. Liu J, Luo Z, Zhang J, Luo T, Zhou J, Zhao X, et al. Hollow mesoporous silica nanoparticles facilitated drug delivery via cascade pH stimuli in tumor microenvironment for tumor therapy. Biomaterials 2016;83:51–65.
32. Yoo J-W, Chambers E, Mitragotri S. Factors that control the circulation time of nanoparticles in blood: challenges, solutions and future prospects. Curr Pharm Des 2010;16:2298–307.
33. Lin Y-S, Haynes CL. Impacts of mesoporous silica nanoparticle size, pore ordering, and pore integrity on hemolytic activity. J Am Chem Soc 2010;132:4834–42.
34. Chen LQ, Fang L, Ling J, Ding CZ, Kang B, Huang CZ. Nanotoxicity of silver nanoparticles to red blood cells: size dependent adsorption, uptake, and hemolytic activity. Chem Res Toxicol 2015;28:501–09.
35. Zhang M, Viennois E, Prasad M, Zhang Y, Wang L, Zhang Z, et al. Edible ginger-derived nanoparticles: A novel therapeutic approach for the prevention and treatment of inflammatory bowel disease and colitis-associated cancer. Biomaterials 2016;101:321–40.
36. Vu-Quang H, Vinding MS, Nielsen T, Ullisch MG, Nielsen NC, Kjems J. Theranostic tumor targeted nanoparticles combining drug delivery with dual near infrared and 19 F magnetic resonance imaging modalities. Nanomedicine 2016;12:1873–84.
37. He Q, Zhang Z, Gao F, Li Y, Shi J. *In vivo* biodistribution and urinary excretion of mesoporous silica nanoparticles: effects of particle size and PEGylation. Small 2011;7:271–80.